Annales
Geophysicae

Global distributions of diurnal and semidiurnal tides: observations from HRDI-UARS of the MLT region and comparisons with GSWM-02 (migrating, nonmigrating components)

A. H. Manson[1], **C. Meek**[1], **M. Hagan**[2], **X. Zhang**[3], **and Y. Luo**[4]

[1]Institute of Space and Atmospheric Studies, University of Saskatchewan, SK, Canada
[2]High Altitude Observatory, NCAR, Boulder, Colorado, USA
[3]Department of Aerospace Engineering Sciences, University of Colorado, Boulder, Colorado, USA
[4]Canada Centre for Remote Sensing, NRCan, Ottawa, Canada

Abstract. HRDI (High Resolution Doppler Interferometer-UARS) winds data have been analyzed in 4°-latitude by 10°-longitude cells at 96 km to obtain the global distribution of the solar-tidal amplitudes and phases. The solstices June–July (1993), December–January (1993–1994), and one equinox (September–October, 1994) are analyzed.

In an earlier paper (Manson et al., 2002b) the emphasis was solely upon the longitudinal and latitudinal variations of the amplitudes and phases of the semidiurnal (12 h) and diurnal (24 h) tides. The longitudinal structures were shown to be quite distinctive, and in the case of the EW component of the diurnal tide there were typically four maxima/perturbations of amplitudes or phases around a latitude circle. In this case they tended to be associated with the locations of the major oceans. Here, a spatial complex spectral analysis has been applied to the data set, to obtain the zonal wave numbers for the tides as functions of latitude. For the diurnal tide the dominant s=1 migrating component and nonmigrating tides with wave numbers s=−3, −2, 0, 2 are identified; and for the semidiurnal tide, as well as the dominant s=2 migrating component, the spectra indicate the presence of nonmigrating tides with wave numbers s=−2, 0, 4. These wave numbers are also simply related to the global longitudinal structures in the tidal amplitudes and phases.

Comparisons are made with the Global Scale Wave Model (GSWM-02), which now incorporates migrating and nonmigrating tides associated with tropospheric latent heat processes, and offers monthly outputs. For the diurnal tide the dominant nonmigrating tidal spectral feature (94 km) is for wave number s=−3; it is relatively stronger than in the HRDI winds, and produces quite consistent structures in the global tidal fields with four longitudinal maxima. Overall, the modelled 24-h tidal amplitudes are larger than observed during the equinox beyond 40° latitude. For the semidiurnal tide,

nonmigrating tides are frequently indicated in the spectra with wave numbers s=−2, 0, 6; and there are complementary longitudinal structures in the global tidal fields with two and four maxima evident. Modelled 12-h tidal amplitudes are much smaller than observed during non-winter months beyond 30°. There is a detailed discussion of the spectral features, their seasonal variations, and the similarities with the HRDI tidal data. This discussion is in the context of the inherent limitations of the model.

Key words. Meteorology and atmospheric dynamics (middle atmosphere dynamics; thermospheric dynamics; waves and tides)

1 Introduction

The observations of the global tides of the middle atmosphere, or "mesosphere lower thermosphere" (MLT), at heights from 60–100 km, have been dominated by sampling from radar systems: Medium Frequency (MF) and "meteor wind" radars. These have provided climatologies with sampling of high temporal resolution (10 days over 365) and altitudes (typically 3 km). Comparisons with models have been both encouraging and challenging, due to the complexity of tidal forcing and propagation processes: examples of such model comparisons have involved the GSWM (Global Scale Wave Model, in 1995 and 1998/2000 versions), and CMAM (Canadian Middle Atmosphere Model), e.g. Hagan et al., 2001; Fomichev et al., 2002; Manson et al., 2002a; Manson et al., 2002b (hereafter Paper 1). However, significant differences have emerged, and a most likely source of these are non-solar-migrating tides or components, since the GSWM is a 2-dimensional model in its basic formulation.

Satellite observations of the tidal field in the MLT region have also been of enormous importance. The winds from the UARS instruments, WINDII (Wind Imaging Interferometer)

Correspondence to: A. H. Manson
(manson@dansas.usask.ca)

and HRDI (High Resolution Doppler Interferometer), gave the first really global views of the tides and have been especially valuable in the upper MLT (95 km and above) and at lower latitudes where the diurnal tide ((1,1) Hough mode) dominates (McLandress et al., 1996).

A note on nomenclature is added here. We use s to refer to the wave numbers of individual tides (or components) which may be propagating or "standing" (zero wave number); the positive sign is for westward propagation. This symbol is used in the majority of papers on the topic of migrating and nonmigrating tides. If more than one tide exists at a given period of oscillation (in this paper, 12 and 24 h only), an amplitude/phase structure is generated around a circle of constant latitude whose number of maxima (we use the symbol S for this) is related to the difference in the wave numbers. If there are only two components present, the number of maxima is equal to the absolute value of the signed wavenumber difference, e.g. Forbes et al. (2003).

Longitudinal variations in the tidal amplitudes and phases, due to the combination of nonmigrating tides and the migrating components, may indeed be large and increasing in importance above 95 km. We mention just two recent studies using UARS winds which demonstrate this: the first considered is the background paper for this present study, and the second also uses HRDI winds but has a different emphasis which proves to be complementary to the present paper. Manson et al. (2002b), or Paper 1, used HRDI winds (between ±70° latitude) for two solstices (June–July 1993; December–January 1993–1994) and an equinox (September–October, 1994), in an analysis based upon small cells (4° latitude, 10° longitude), and showed that at 96 km the diurnal tide (EW, east-west, component) has rather clear maxima over the oceans. The semidiurnal tide has much less longitudinal variation or structure. This present paper builds upon that study by calculating the zonal wave numbers of the nonmigrating semidiurnal and diurnal tides, as described below. Secondly, Forbes et al. (2003) used HRDI and WINDI daytime and night-time "95 km" winds (December 1991–September 1994) to identify several diurnal tides: the eastward propagating tide with zonal wave number s=−3, the "standing" (s=0) oscillation, and the westward propagating s=2 tide. They also showed that this combination of tides leads to significant longitudinal variations in tidal structure between ±40° latitude. The s=−3 tide near the equator was associated with the Kelvin wave (a symmetric mode) in the Northern Hemisphere's (NH) summer/fall, and with the enhanced presence of an antisymmetric mode during October–April; the s=0 existed for most months, was nonsymmetric in amplitude about the equator (SH maxima), and was consistent with an antisymmetric mode and its superposition at times with a symmetric mode; and the s=2 was consistent with a symmetric mode in combination with modest contributions from an antisymmetric mode, and exhibited strong and seasonal changes. There were supportive GSWM studies and comparisons. Forbes et al. (2003) noted they elaborated or "built" upon a study by Talaat and Lieberman (1999). The latter study used daytime HRDI wind and temperature data

for the first time for this tidal purpose, and provided vertical structure. However, they noted that there were issues with aliasing. Comparisons of our results with Forbes et al. (2003) are interesting, as the analysis methods (Sect. 2) are somewhat different, and the focus of our study (relationships between the nonmigrating tides and the global tidal structures) differs; we also assess the semidiurnal tides.

Ground-based radar studies are also beginning to contribute information on longitudinal variations as the number and distribution of MF and meteor wind radars expands. Jacobi et al. (1999) assessed the variation of the semidiurnal tide using a chain involving Europe, Russia and Canada (longitudinal tidal amplitude structures were inferred in winter, with one maximum along the latitude circle, S=1); and Pancheva et al. (2002) used a massive 22 radar network during summer (1999) and demonstrated the structure number S=1 in the diurnal tide amplitudes. Finally, the new CUJO network (Canada, U.S., Japan Opportunity) of MF radars has demonstrated that the variations in tidal and planetary wave climatologies (70–95 km) found between London (43 N, 81 W), Platteville (40 N, 105 W) and Wakkanai (45 N, 141 E), a 7000 km longitudinal sector, are very significant and often larger than local latitudinal variations (12–14° changes) (Manson et al., 2004a) Tidal wave number analysis provided nonmigrating tides components with wave numbers s=2, 0 or 3, and 4 for the diurnal and s=1, 0 or 3 for the semidiurnal.

The basis for modelling the nonmigrating tides is longitudinally varying forcing, which thus far has involved tropospheric water vapour, e.g. Forbes et al. (1997). Discussion below focuses briefly on the enormous efforts made in this regard. It is expected that this will have a major impact upon the diurnal tides, and a lesser impact upon the semidiurnal tides. A similar effort based upon longitudinally varying ozone distributions, e.g. from the Odin satellite (Llewellyn, 2002), can be expected to impact the modelling of the semidiurnal tide in the future.

Forbes et al. (2003) discuss the role and analysis of global cloud imagery data, which is related to deep convective activity and which can be converted to rainfall rate and latent heating (Forbes et al., 1997). (We occasionally use the abbreviation TLH, tropospheric latent heat, to categorize this hereafter.) It is important to mention the forcing mechanisms here, as the identification of particular wave numbers later in the paper then has a physical justification. Also, given the large number of tidal papers now emerging on this theme, a brief summary of these is useful for the reader. The Forbes et al. (2003) paper is elegantly tutorial in nature, and is most instructive with regard to those new developments. They note that the strongest spectral power for TLH lies at wave numbers −3, 1, 5 for the diurnal tide and −2, 2, 6 for the semidiurnal tide. Significantly, the migrating s=1, 2 tides are also strongly forced by the TLH processes. They explain that modulation of solar energy absorption by the dominant topographic structures at low latitudes (structure numbers, S=4, 1) leads to these tidal components (s±S), and also to s=0, 2 for the diurnal tide. Other heating mechanisms,

such as insolation absorption by longitudinally varying water vapour, will generate additional nonmigrating tides (Forbes et al., 2001). Finally, nonlinear interactions between the stationary planetary wave (wave number 1) and migrating tides also leads to s=0, 2 for the diurnal tide (modelling exercise; Hagan and Roble, 2001), and to s=1, 3 for the semidiurnal tide (UARS winds; Angelats i Coll and Forbes, 2002). The existence of such tides (or components), and the related global longitudinal structures in amplitude and phase within the MLT, depend upon a myriad of factors, which indeed reflect upon the importance of studying tidal activity within the lower and middle atmospheres. At this stage it is useful to remind the reader that Forbes et al. (2003) did detect s=−3, 0, 2 for the diurnal tide within the MLT, using UARS winds, consistent with tropospheric latent heat forcing (and perhaps the standing planetary wave process).

Finally, some comments upon the GSWM modelling efforts, which have now incorporated the tropospheric latent heat forcing, are appropriate. The so-called GSWM-02 model will be described later in Sect. 2, and it basically incorporates the GSWM-00 radiational tides resulting from non-longitudinally varying forcing (Hagan et al., 2001) and the tides (nonmigrating as well as the migrating) forced by tropospheric latent heat processes. This present paper is one of the first to use the new "combined" model, which makes the comparisons with the tides from HRDI particularly useful. Two recent significant papers which have used the GSWM to assess the MLT tides excited or forced by tropospheric latent heat processes only are Hagan and Forbes (2002) for the diurnal tide, and Hagan and Forbes (2003) for the semidiurnal tide. They incorporate 7 years of global cloud imagery data, to provide a "climatology" with monthly resolution. Brief comments are appropriate. The first remark is that GSWM-02 will contain the same tides/components as those incorporated and discussed by these two papers, although they will necessarily be a smaller part of the total tide. Also, the global longitudinal structure (as described by the structure number, S) of the total tide may differ from those shown in the two papers due to phase constructive/destructive interference. For the diurnal tide, Hagan and Forbes (2002) demonstrate the strong importance of s=−3, −2, 0, 2 non migrating components, and the migrating s=1, in determining the global tidal field above 90 km. The complementary paper on the semidiurnal tide, as described by Hagan and Forbes (2003), demonstrates more complexity at MLT heights, with non migrating tidal responses at all latitudes (rather than dominantly lower latitudes for the diurnal tide.) Components s=−3, 0, 1, 2, 3, 5, 6 may be significant. Also, monthly responses for the diurnal and semidiurnal tides differed, and interannual variability is expected. It will be useful, therefore, in this paper, to assess the relative contributions of the migrating and nonmigrating tides in GSWM-02 for the first time and to compare these with the HRDI tidal field.

The contributions to our knowledge of nonmigrating tides in the MLT which will be provided in this present paper have been mentioned in the above paragraphs. However, and to summarize, the paper will assess aspects of the total tidal winds for the diurnal (Sect. 3) and semidiurnal (Sect. 4) tidal harmonics, using the HRDI (∼96 km) data and analyzed results of Paper 1, along with matching "data" and analysis from GSWM-02. In each case spatial spectral analysis has been applied to obtain the amplitudes and phases of the zonal wave numbers of the migrating and nonmigrating components, and then these are compared with the global structures (amplitudes and phases) of the tides. Some comparisons between middle atmosphere climatologies from the GSWM-02 and radar data are shown for completeness in each section.

2 Data analysis

We provide brief descriptions here as the original papers referenced above have richer descriptions. Regarding HRDI, the data files from Paper 1 were used directly. At each 4° by 10° (latitude/longitude) area or cell, time sequences of the HRDI winds for the respective two month intervals were reformed into 24-h mean days only, according to their local time of day. After that, harmonic fitting was applied to the mean-day data, to obtain the mean winds, and the amplitudes and phases of the 24- and 12-h tides. When the time coverage of the mean-day data was larger than 15 h for a day, the mean wind and 24-h and 12-h oscillations were all fitted. However, when data yield was low (<16 h, but >8 h), typically above 50° due to the lack of day-time or night-time data, depending upon the local time of the UARS orbit, only 12-h fitting was accepted. Similar criteria in the analyses of radar data have been shown to be appropriate by us in using MF radars (unpublished) and by Jacobi et al. (1999). Also at the higher latitudes, where the 12-h fitting was done, the 24-h tidal amplitudes are known to be small, and so is the related error. The 12-h only fitting was useful from 45–70° in NH and SH summers. Excellent consistency occurs between neighbouring cells for amplitude and phase (Paper 1). Full global grids of latitudes and longitudes, with land images, are used for the contours of amplitudes and phases. Estimates of significance suggest that amplitudes less than 5–10 m/s are noisy, and this is confirmed by inspection of the phase contours, which show more random phases in these regions.

Following the comments on GSWM in the Introduction, some basic description is appropriate. The GSWM is a 2-dimensional, linearized, steady-state numerical tidal and planetary wave model which extends from the ground to the thermosphere (Hagan et al., 2001, http://www.hao.ucar. edu/public/research/tiso/gswm/gswm.html). Briefly, GSWM tidal and planetary wave predictions are solutions to the linearized and extended Navier-Stokes equations for perturbation fields with characteristic zonal wave numbers and periodicities that are specified along with the zonal mean background atmosphere. Mean zonal winds are included. The most recent version of the GSWM tidal model, GSWM-02, includes the GSWM-00 results (e.g. Hagan et al., 2001), along with the migrating and nonmigrating diurnal and semidiurnal tides that are excited by tropospheric latent heat processes in the tropical troposphere (Hagan and Forbes,
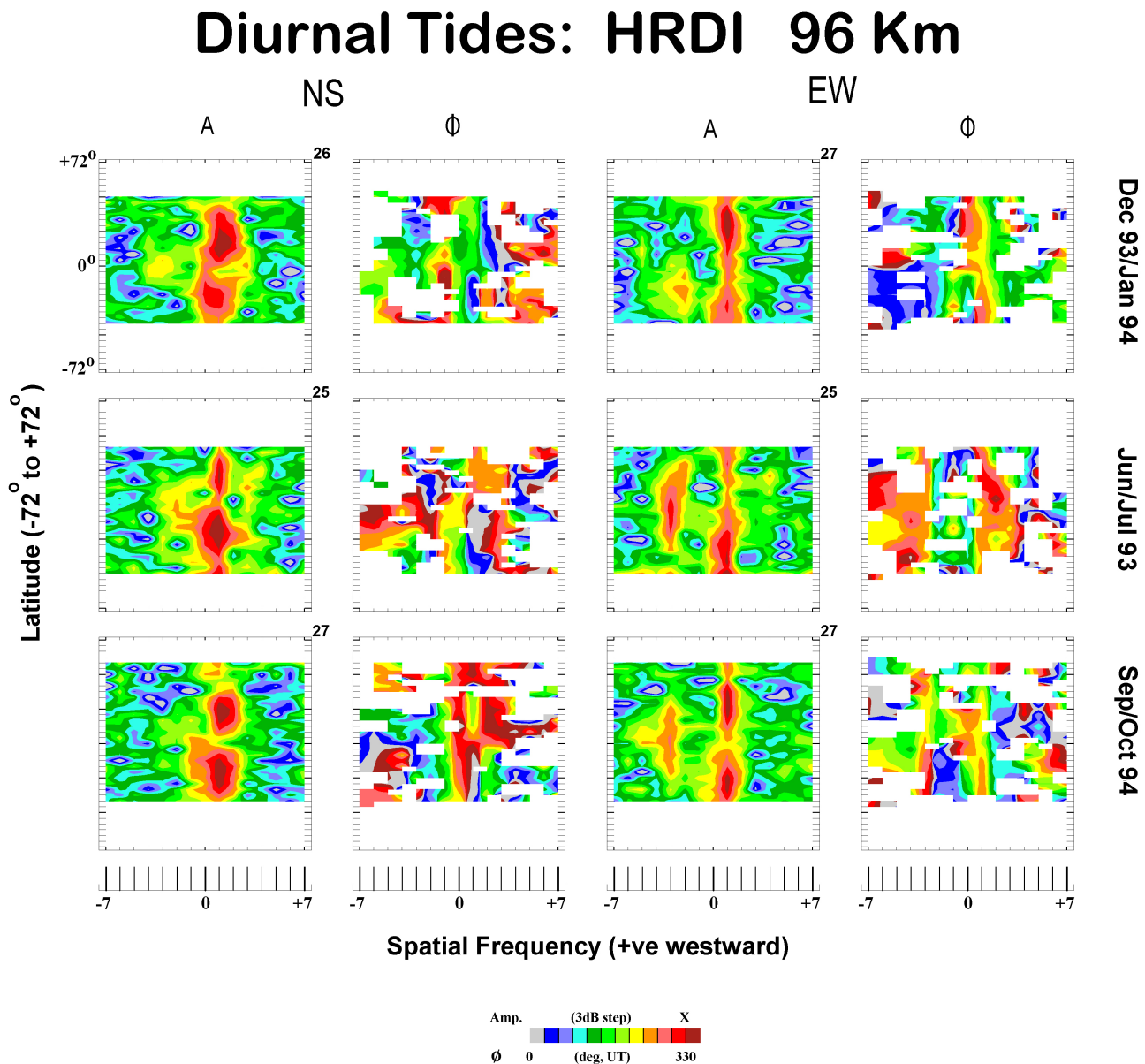
Diurnal Tides: HRDI 96 Km

Fig. 1. Spatial spectral analysis of the global HRDI complex diurnal wind field, providing wave number versus latitude contours of amplitude and phase. Positive (+)/negative (−) numbers represent westward/eastward propagating "tides" or "components". The amplitude colour scale is in dB (decibels) where dB=$20 \log_{10}$(RMS m/s); the dB value for the red colour for each portion of the Figure are provided. The phases are in degrees relative to the UT=0 h longitude, so that each colour represents a change in phase of 30° (or 2 h of local time). Values are used for contouring when the amplitude is greater than the value of the second bin (see text for further details). Contour plots for each component of the wind (NS, north-south; EW, east-west) and for two solstices and one equinox are provided.

2002; 2003). Briefly, the GSWM-00 results are the monthly variable migrating tidal responses to the absorption of solar radiation throughout the atmosphere. The GSWM-02 results also include the "standing" (wave number 0) diurnal and semidiurnal tidal oscillations along with eastward and westward propagating harmonics with wave numbers between 1 and 6 inclusive. Because the nonmigrating tides beat with the migrating diurnal and semidiurnal tides, the GSWM-02 monthly tidal climatologies vary with longitude.

The plots of global tidal structures for diurnal and semidiurnal harmonics (Figs. 2, 4, 7, 9), and for either HRDI or GSWM-02 data, are formed from the phases or amplitudes for each available cell. Contours are formed as described in Manson et al. (2003), but a brief explanation is also given below in the paragraph on the MF radar analysis, since the methodology is the same for both. Each plot has amplitudes according to a colour scale; the values in m/s for the red colour, and the increments for each colour, are provided. Global maps are added to each figure to aid in locating the structures.

If data existed at all longitudinal cells for a particular latitude (the cells are 4° in latitude, 10° in longitude), spatial complex spectral analysis has been applied to the longitudinal sequence of complex tidal values (from Manson et al., 2002b) for each tide (24 h, 12 h). In contrast, the cells used by Forbes et al. (2002) were 30° in longitude. Solutions have been sought for the zonal wave numbers s=0 to s=±7, with +ve being westward propagating. Migrating and nonmigrating tides are present in this analysis, unlike Forbes et al. (2002), who first removed the migrating components. Contours of amplitudes and phases are then formed (Figs. 1, 3, 6, and 8), as described in the paragraph below. Amplitudes are provided in decibels (dB) to provide the best range of colours over the amplitude ranges; in each case the dB value for the largest amplitude/colour range is provided to allow for intercomparisons (dB=$20 \log_{10}$(RMS amplitude)). For clarity, and to remove noisy values, phases are only plotted when the corresponding amplitudes are at least two amplitude contour levels above the minimum.

Data from the Saskatoon MF radar have been exhaustively explained elsewhere, e.g. Manson et al., 2003. The monthly tidal analysis uses a least-squares fit of a mean, 24-h and 12-h oscillations, to a composite monthly day in which the squared error is weighted by the number of raw (5 min) values in each composite hour. As in the tidal papers referenced earlier, there must be data in at least 16 of the possible 24 composite hours. (At most heights there are typically at least 20 h of data; and analysis experiments in which the number of hours with data are reduced to 16 show that the fitting results are still quite robust.) The tidal contours cover 6 heights and 12 months. There is no smoothing. The methodology for contouring that is now described is the same for all three types of figures in the paper. Interpolation between data points employs a "bilinear patch" method, viz. the interpolated value is ax+by+cxy+d, where a, b, c, d are solved from the corner values in the grid (of data points). In the case of phase contours, and provided that the four corner phases have a spread of less than 180°, two separate BLP calculations are done, one for cosine and one for sine. The resulting pair of interpolated values at each point is recombined to get its phase value. Any pixels in the amplitude plots representing a value greater than the maximum in the legend are set equal to the maximum. Finally, MF radar data for which the heights are expected to be inaccurate, due to virtual versus real height considerations, are not used. This leaves gaps at the greatest heights in summer. Five heights of the Global Scale Wave Model (GSWM-02) have been plotted on the same scale to provide comparisons with the observations.

3 Diurnal Tides

3.1 HRDI global tides at 96 km

Following Paper 1, where the global tidal structures were provided for the solstices of December–January (1993–1994), June–July (1993), and September–October (1994),

the complex spatial frequencies appropriate to the global tides are now provided and discussed. The analysis method was described in Sect. 2, and is a complex spatial spectral analysis providing amplitudes and phases of spatial frequencies (wave numbers) from 0 to ±7 versus latitude. The wave numbers represent tidal "components" or "tides", where +ve is westward and −ve is eastward (Fig. 1).

The dominant amplitude features are a broad contour centred on s=1 (the solar migrating tide), and having amplitude within 10 dB (a factor of 3.2 from dB=$20 \log_{10}$ (RMS amplitude)) of the maximum from approximately s=0 to 2. Also, the s=−3 contours are relatively strong (yellow to red) in one wind component or the other, for each season. Table 1 summarizes the wave numbers of the nonmigrating tides represented, and these also include s=−2, 3, 4. There is some seasonal variability. From the Introduction, nonmigrating tides related to topographic forcing (structure numbers 4, 1) would include s=−3, 5 and 0, 2. The latter two would also be forced by nonlinear interactions with a standing planetary wave of wave number 1; while a planetary wave of wave number 2 would force s=−1, 3. The existence of such tides in the MLT depends upon many factors, and as evident from Table 1, a number of these components are observed.

It is also useful to relate the dominant wave numbers of Table 1 and Fig. 1 to the (amplitude/phase) longitudinal structures or patterns in the global diurnal tides (as also shown in Paper 1). To aid in this comparison we show (Fig. 2) contour plots for both components of the tides for the three seasons in slightly different (more compact) format, but one that matches Fig. 1. The distributions of land masses and oceans are shown below each column of plots, to enable any topographic or regional linkages to be made; the dominant topographical features at lower latitudes have "wave numbers" of 1 and 4 (Yagai, 1989). Structure numbers (S) of the tidal structures in Fig. 2 for both the amplitudes and phases range from 1 to 4, and have been added to Table 1; these are clearest in the EW component for all three seasons, where S values of 3 and 4 are especially evident. These have been obtained from visual inspection of the tidal structures, since the relationships between strong features in the wave number spectra and the tidal structures (as discussed below) should be clearly evident. There is also some indication of association of these amplitude and phase structures with the oceanic positions for the EW component (this is perhaps more evident in the colour choices and larger format used in Paper 1). This association is to be expected, as latent heat processes associated with deep convection activity vary between the oceans and continents.

As shown by Angelats i Coll and Forbes (2002), the number of maxima in a longitudinal structure or pattern of tidal amplitudes (structure number, S, in this paper) is given by the difference between the wave numbers of the tides that are present. For example, in June/July the s=−3, 1 components dominate in the EW wind spectra (Fig. 1), which should provide the structure number S=4 in the tidal patterns. Indeed, 4 maxima are clearly evident in the appropriate amplitude and phase plots of Fig. 2. In general, the numbers of maxima in

Table 1. Summary of HRDI Tidal Components: Diurnal.

HRDI	NS Wind			EW Wind		
December–January 1993/94		1[a] −3			1[a] −2	
		(1 longitudinal structure)[c]			(3 longitudinal structures)[c]	
June–July 1993	3	1[b] −2		4	1[b] −3	
		(3, 2 longitudinal structures)[c]			(4 longitude structures)[c]	
September–October 1994		1[a]			1[a] −3	
		(1 longitudinal structure)[c]			(4 longitudinal structures)[c]	

[a] Broad feature 0–2, both hemispheres, especially NS component; phases distinguish components m=0, 1, 2 modes.
[b] Broad feature 0–2, winter hemisphere, especially NS component; components (m=0, 2) less well distinguished.
[c] HRDI amplitude and phase contours (Fig. 2).

Table 2. Summary of GSWM-02 Tidal Components: Diurnal.

GSWM	NS Wind				EW Wind			
December/ January	4[D]	1[a]	−2[W]	−3	4[D]	1	−2[W]	−3
		(4 southern structures)[b]				(4 structures)[b]		
June/July	4[J]	1[a]	−3		4[J]	1	−3	
		(2, 4 structures)[b]				(2, 4 structures)[b]		
September October	4[S]	1[a]	−2		4[S]	1	−3	
		(little structure)[b]				(4 structures)[b]		

[a] Broad feature 0–2; phases do not distinguish m=0, 1, 2 components.
[b] GSWM-02 amplitude and phase contours (structures) of Fig. 4.
D-December   J-June   S-September   W - Weak.

the structures (S values) evident from Fig. 2 are consistent with the dominant components or tides evident in Fig. 1 (and Table 1). There are two interesting cases where the spectral features centered on s=1 are very broad (NS, December/January and September/October), suggesting that weaker s=0, 2 components could also be present. If so, the expectation is for S=1 to dominate the global or longitudinal tidal structures, and that is indeed the case, as shown in Fig. 2.

Now consider the phases of the components or tides of Fig. 1/Table 1. Here, phase values are used for contours if the corresponding amplitude values are above the value of the second colour bin, to minimize noisy contours. For all three seasons the dominant migrating tide (s=1) evidences close to zero phase differences for the EW component across the equator (for latitudes near and less than 24°), and large phase differences (5–6 colour changes, 10–12-) for the NS component. This is also evident in the global tidal structures plots (Fig. 2), since at the equator the continuous/discontinuous nature of the colour contours for the EW/NS components is evident, despite the modulation of the pattern by the nonmigrating tides. Notice also that the amplitudes for s=1 maximize near 24° (both hemispheres). This behaviour is consistent with the symmetric (1, 1) Hough tidal mode.

For the s=−3 tide, maximum EW amplitudes (Fig. 1) occur in June/July and September/October for which the phase is continuous across the equator, or with a modest phase shift (2–3 colours, 4–6 h), respectively. NS amplitudes are barely discernable (−15 dB) and were not scaled for Table 1. This is consistent with the symmetric Kelvin wave (Forbes et al., 2003; Talaat and Lieberman, 1999). In contrast, during December/January this s=−3 component is only evident in the NS amplitudes, and it does not demonstrate a phase shift across the equator. Such behaviour was also noted by Forbes et al. (2003) in a larger set of HRDI/WINDII data, who suggested the greater influence of the first antisymmetric tidal mode between October and April. (This mode is forced by direct tropospheric heating.)

Finally, some comments on the s=0 and 2 nonmigrating tides are useful. Careful inspection of the phases in Fig. 1, but bearing in mind that some phase contours are associated with very small amplitudes, indicate that there are distinctive values for these wave numbers. For s=0, the amplitudes are larger for the NS component and in the Southern Hemisphere (SH), and the phases are continuous (or show small changes) across the equator. The tide of the EW component is smaller, with noisier phases, although the December/January season

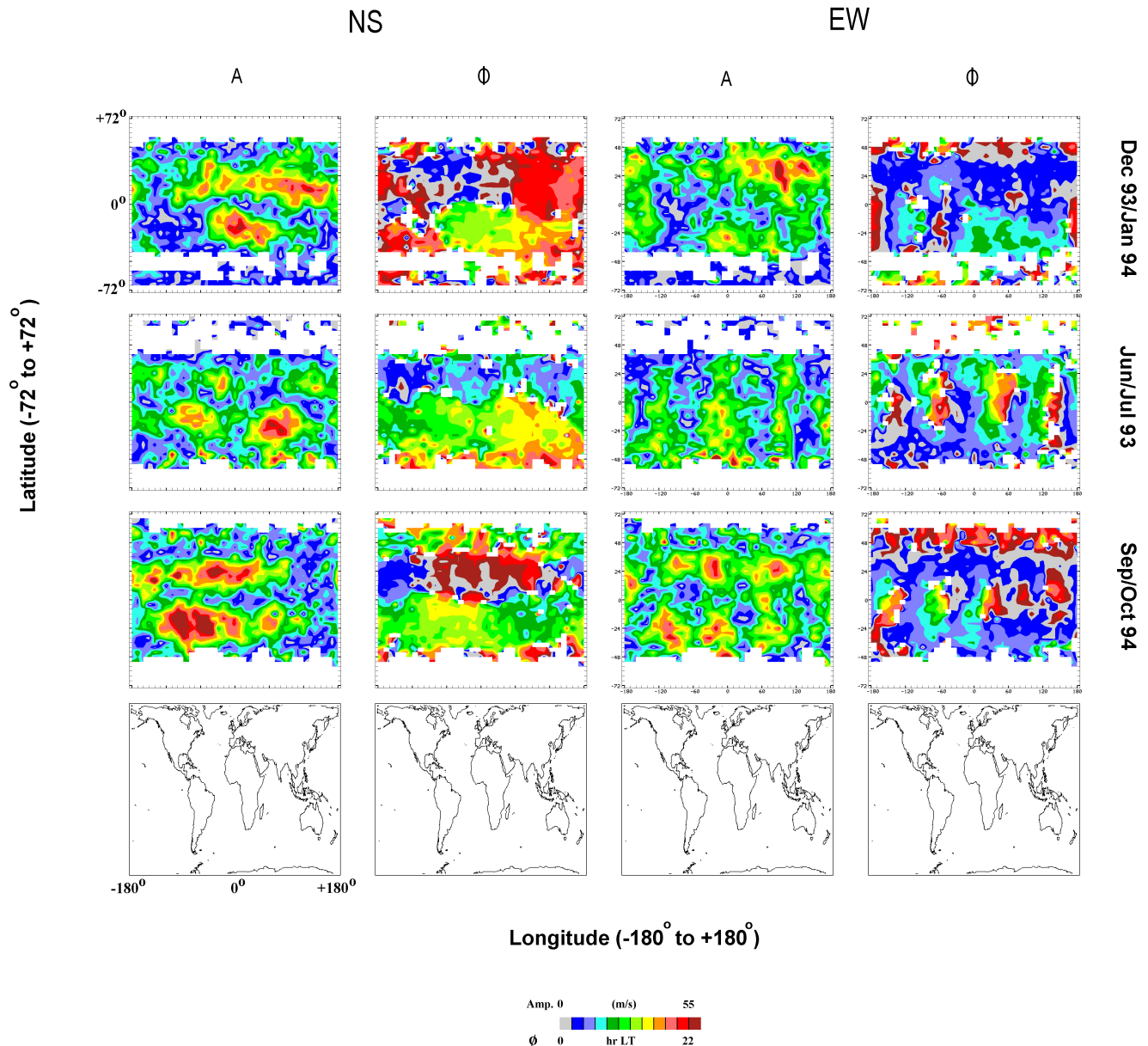# Global HRDI Tidal Structures: Diurnal 96 Km

Fig. 2. Global HRDI tidal structures for the diurnal tide at 96 km, as functions of latitude and longitude, and for NS and EW winds. As in Manson et al. (2002b), the amplitudes and phases refer to cells of size 4° (latitude) by 10° (longitude). The amplitude colour scale is in m/s, and the phases are in hours (local solar time). The amplitude value in m/s of the red colour is provided, and the amplitude increment for each colour is 5 m/s. Contour plots for two solstices and an equinox are provided.

shows a clear phase change of ∼12 h across the equator. As also suggested by Forbes et al. (2003), this is consistent with the fundamental antisymmetric mode (they also suggested the additional presence of the symmetric mode leading to destructive interference in the NH). Finally, for s=2, the phase changes across the equator are smaller or zero for the EW component and are larger (5–6 colours, ∼12 h) for the NS component. This is suggestive of a dominant symmetric

mode (Forbes et al., 2003). Overall there is good agreement between our analysis and that of Forbes et al. (2003), even though the data sets and analysis differ somewhat; however, we have also shown the relative strengths of the migrating and nonmigrating tides and the resulting standing wave patterns in the global tidal structures. We follow this with a similar presentation based upon the GSWM-02 tidal values.
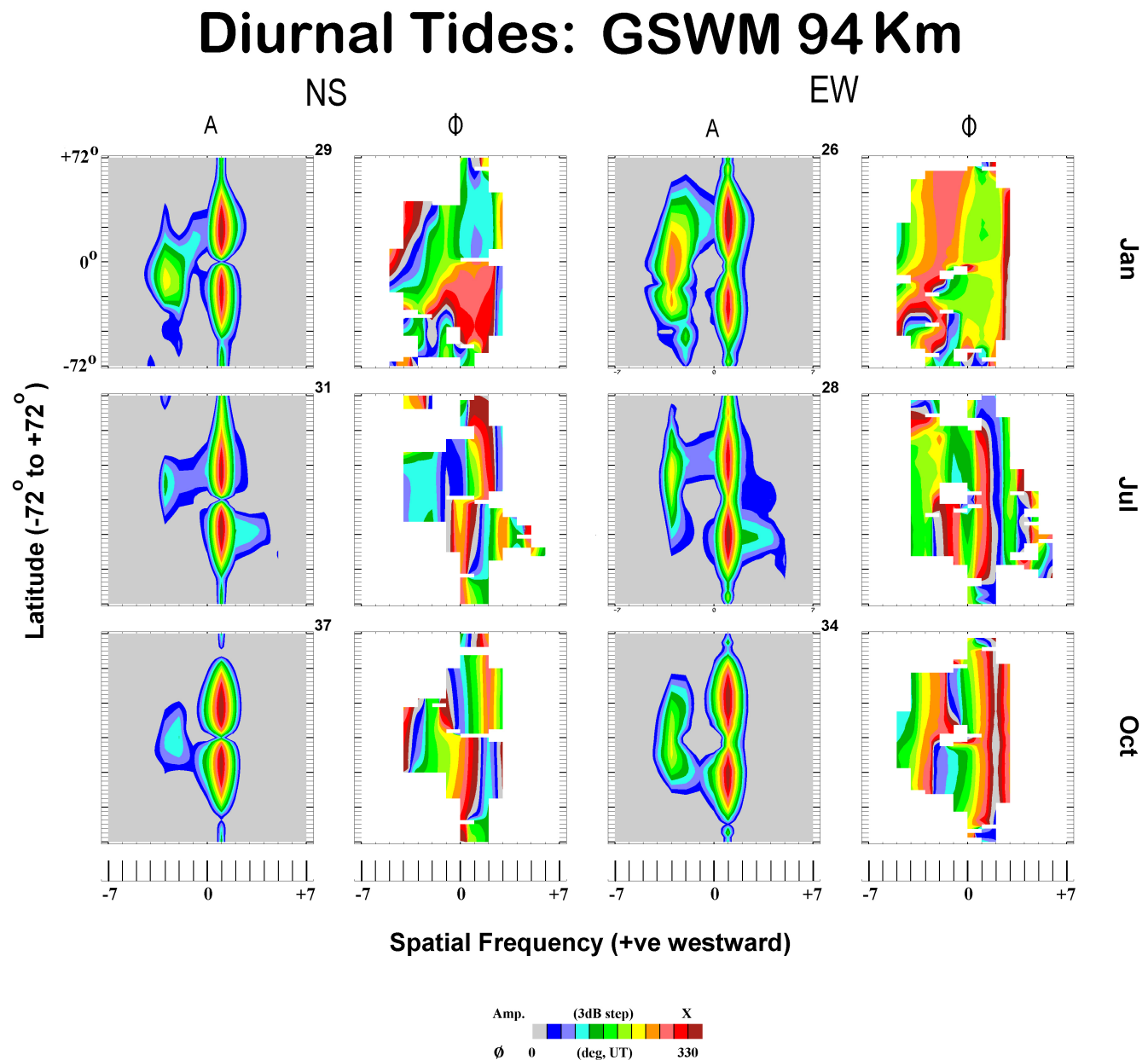
Diurnal Tides: GSWM 94 Km

Fig. 3. Spatial spectral analysis of the global GSWM-02 complex diurnal wind field, providing wave number versus latitude contours of amplitude and phase. Positive (+)/negative (−) numbers represent westward/eastward propagating "tides" or "components". Otherwise, the description is as for Fig. 1.

3.2　GSWM-02 global tides at 94 km

The development of the GSWM (1998, 2000) versions (hereafter GSWM-00), to now include nonmigrating and migrating tides associated with the release of latent heat within deep convective clouds (Sect. 2), provides an excellent opportunity for comparisons with our analysis of HRDI data. These will aid in the assessment of the realism of the model and whether further changes and forcings are required. Here we have formed figures of the same format as the previous section, that can be directly compared with observations. Figure 3 provides the spatial spectral analysis of the global

GSWM-02 complex diurnal wind field. Contours of amplitudes and phases are again plotted as functions of wave number and latitude. We have chosen to show one of the months for each of the three bimonthly seasons of HRDI data, since the changes for neighbouring months in these three seasons within GSWM-02 are usually modest with regard to the existence of major spectral features. However, the tabulations of Table 2 are based upon examination of both months in each of the seasons, for generality. The amplitude similarities with Fig. 1 and Table 1 are quite strong: there are strong, rather broad spectral features centred on s=1 for all plots; and clearly evident features centred on s=−3 for the three seasons
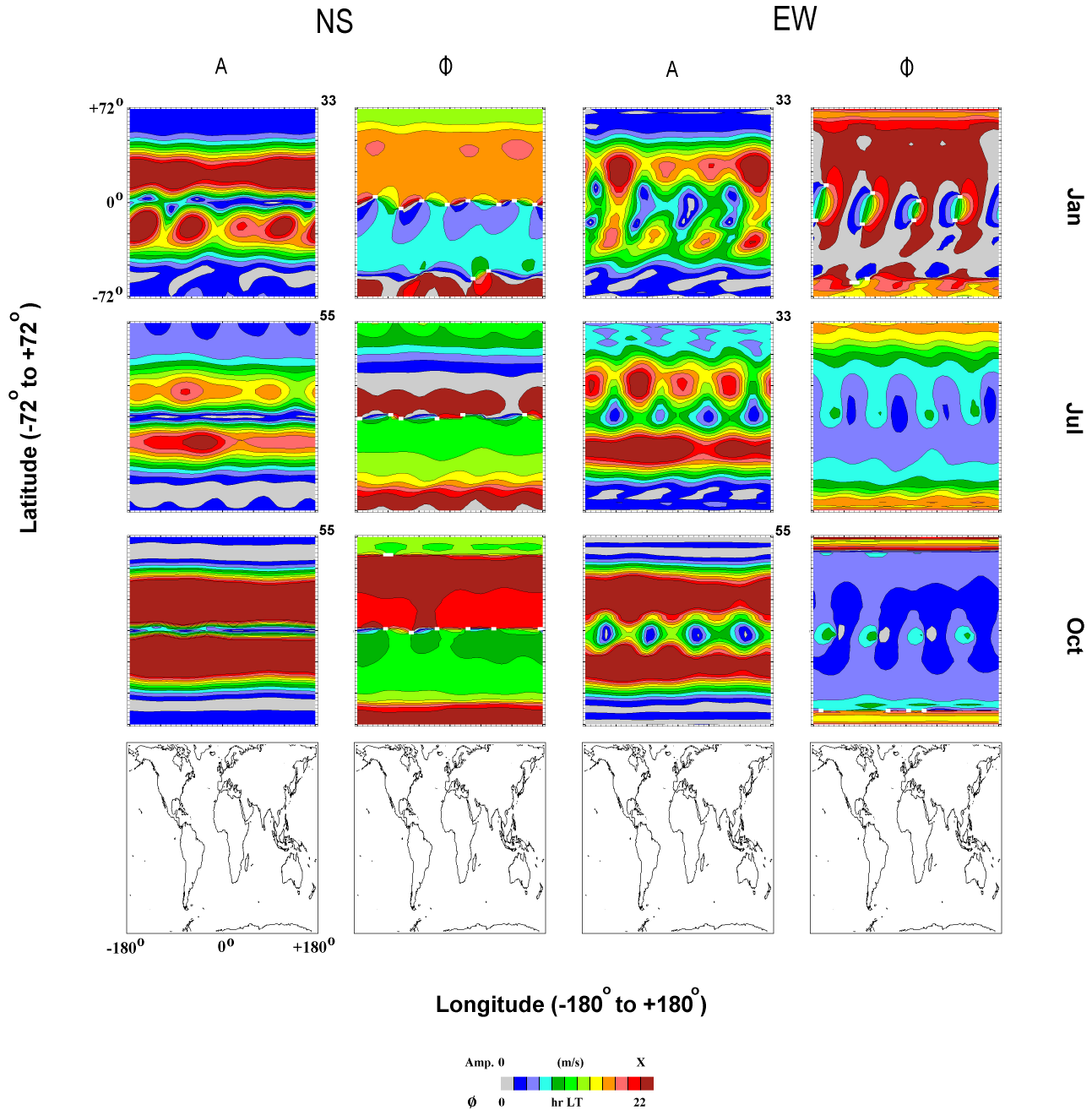
Global GSWM Tidal Structures: Diurnal 94 Km

Fig. 4. Global GSWM-02 tidal structures for the diurnal tide at 94 km, as functions of latitude and longitude, and for NS and EW winds. The amplitude increments for each colour are 3 or 5 m/s. Otherwise, the description is as for Fig. 2.

(June and July (EW), September and October (EW) and December and January (NS)). Differences are that the features at s=1 are not as broad as observed by HRDI (and rarely extend to s=0, 2 with any significant amplitude); the spectral features at s=−3 are more consistently modelled than observed (features are evident in January and December (EW), and July (NS) and several months other than the six being specifically dealt with here); and the s=4 spectral features are

consistently modelled (e.g. the alternate months, December, June, and September included in Table 2), but only observed in June/July (EW).

Moving to the global GSWM-02 tidal structures (Fig. 4), the effects of the differences in the modelled and observed spatial spectra of the tides are immediately evident. While structure number S=4 (numbers of maxima in the amplitude/phase) was evident in only two amplitude-phase pairs

for HRDI (June/July, September/October; EW component), it is dominant in four of the pairs for GSWM (January, NS and EW; July and October, EW component). A summary of the numbers of amplitude maxima (and/or phase perturbations) are provided in Table 2, and these structure numbers S (S equalling the difference in the dominant wave numbers) are consistent with the wave numbers of the dominant tidal components. As noted in the consideration of the HRDI data, the topographic feature with "wave number" 4 will have a strong input with respect to the forcing of the tides which are associated with the tropospheric latent heat. Oceanic structures are related to this topography. Thus, there is a tendency for the amplitude maxima and related phase features in Fig. 4 to be located in the oceanic regions (Eastern Pacific, Atlantic, Indian and Western Pacific), but there is seasonal variation in those positions. This is at least partly associated with the presence of other spectral maxima ($s=-2$, 4) in GSWM-02, which have led to further modulation of the longitudinal structures.

Now consider the spectral phases of the tides or components in Fig. 3 and Table 2. Here a value is used for contouring when the amplitude is greater than the second colour bin, or the neighbour of such a value, regardless of its amplitude. For the migrating $s=1$ tide the phases for EW/NS components are, respectively, continuous or demonstrate $180°/12$ h changes across the equator in each of the three seasons. The global tidal structures (Table 4), which are also dominated by this tide (albeit modulated by the $s=-3$ tide), also demonstrate this tidal phase behaviour, which, along with the amplitude maxima near $24°$, favours the dominance of the (1, 1) Hough tidal mode again.

Consistent with the narrow amplitude feature at $s=1$, the phases of Fig. 3 do not show any differential structure in the regions of $s=0$, 2, suggesting that the influence of these tides is very weak in the new combined GSWM. (There is merely the expected continuous sweep of frequencies as one views from $s=0$ to $s=2$.) In the earlier study by Forbes et al. (2003) GSWM was forced by the appropriate Hough modes (e.g. wave numbers 0, 2) and then normalized to match the HRDI observations. Also, Hagan and Forbes (2002) in their assessment of MLT tides solely forced by deep convection processes in the lower atmosphere, showed that amplitudes for $s=0$, 2 were typically 10–20 dB (3 to 10 times) weaker than the migrating (non radiationally forced) tide in the 95 km height region. In the GSWM used here the amplitude ratios will be even greater as the radiational migrating mode is now also included.

Another factor is the absence of nonlinear wave interactions in GSWM, in particular the standing planetary wave of wave number 1, which would potentially lead to nonmigrating tides with wave numbers $s=0$, 2.

Considering the relatively strong $s=-3$ tide, phase changes across the equator for the EW component are quite small in July but are typically 4 h for neighbouring months (not shown). The amplitudes for the NS component are typically smaller for these months (for several months the values are in the lowest colour bin) and the phases are often not

present in the plot. However, based upon the EW component, and as for the HRDI tides, the symmetric Kelvin wave is often favoured. For January, and the neighbouring months including autumn, the phase shift across the equator is larger (~4–6 h) for the EW and the NS components (when the low-amplitude phase values are cautiously scrutinised) which, as for the observed HRDI tides, suggests more influence of the antisymmetric tidal modes. The two non-summer months of Fig. 3 (January, October) are quite typical.

Although the main focus of this paper has been the non-migrating tides, the tides forced by tropospheric latent heat processes, and the comparison of the spectral wave numbers (spatial frequencies) from global observations and models, it is appropriate to take this opportunity to compare the general features of the global tidal structures as represented by HRDI and GSWM-02.

The phases (colours) change strongly with the three months/seasons for each wind component in Fig. 4 (GSWM), and somewhat less in Fig. 2 (HRDI). There are fair agreements in the relative colours, indicating some similarities in tidal phases between the observations and the model. The amplitudes are quite easy to infer from the figures: each figure or section thereof has a specific maximum amplitude to provide optimum colour ranges for each global image, and the values (m/s) of the last red shade are added to the top right corner of each contour plot. Equinoctial maxima in GSWM-02 are strong compared even to HRDI, as expected from GSWM-00 (Manson et al., 2002a, b). There, the agreements between the 24-h tides of the MF radar, and the GSWM-95 and GSWM-00 versions, were shown to be very encouraging. However, here, at the higher mid-latitudes and above 85 km, the GSWM-02 equinoctial values are larger than the earlier versions and warrant further assessment.

Hence, we show in Fig. 5 the GSWM-02 climatologies of the MLT for the latitude and longitude ($51°$ N, $105°$ W) closest to that of Saskatoon ($52°$ N, $107°$ W), which is the site of the MF radar that the Canadian authors have operated for two solar cycles. Here, a 7-year vector average of the mean monthly days (from each year) has also been calculated (1995–2002) for the radar data. Indeed, in the new model, the large equinoctial amplitudes (circa 20 m/s at 94 km) and the related and consistent monthly short vertical wavelengths have become a strong feature of $51°$ N.

Such large amplitude modelled features were more typical of $39°$ N within GSWM-00, as shown in the comparison between the Platteville ($40°$ N, $105°$ W) and Saskatoon climatologies (Manson et al., 2003). In GSWM-95 these features of strong equinoctial amplitudes and short vertical wavelengths were even more restricted to the low latitudes (Manson et al., 2002a). Although GSWM-02 has longitudinal variations, these are fairly modest at $50°$ and northward (Fig. 4), so that at no longitudinal location do characteristics exist which are similar to those observed (Fig. 5).

We note in conclusion that the well-known speed bias of MF radar-derived winds would change the colours/speeds within Fig. 5 modestly. Very intensive comparisons between climatologies from MF and Meteor-Wind radars in Northern
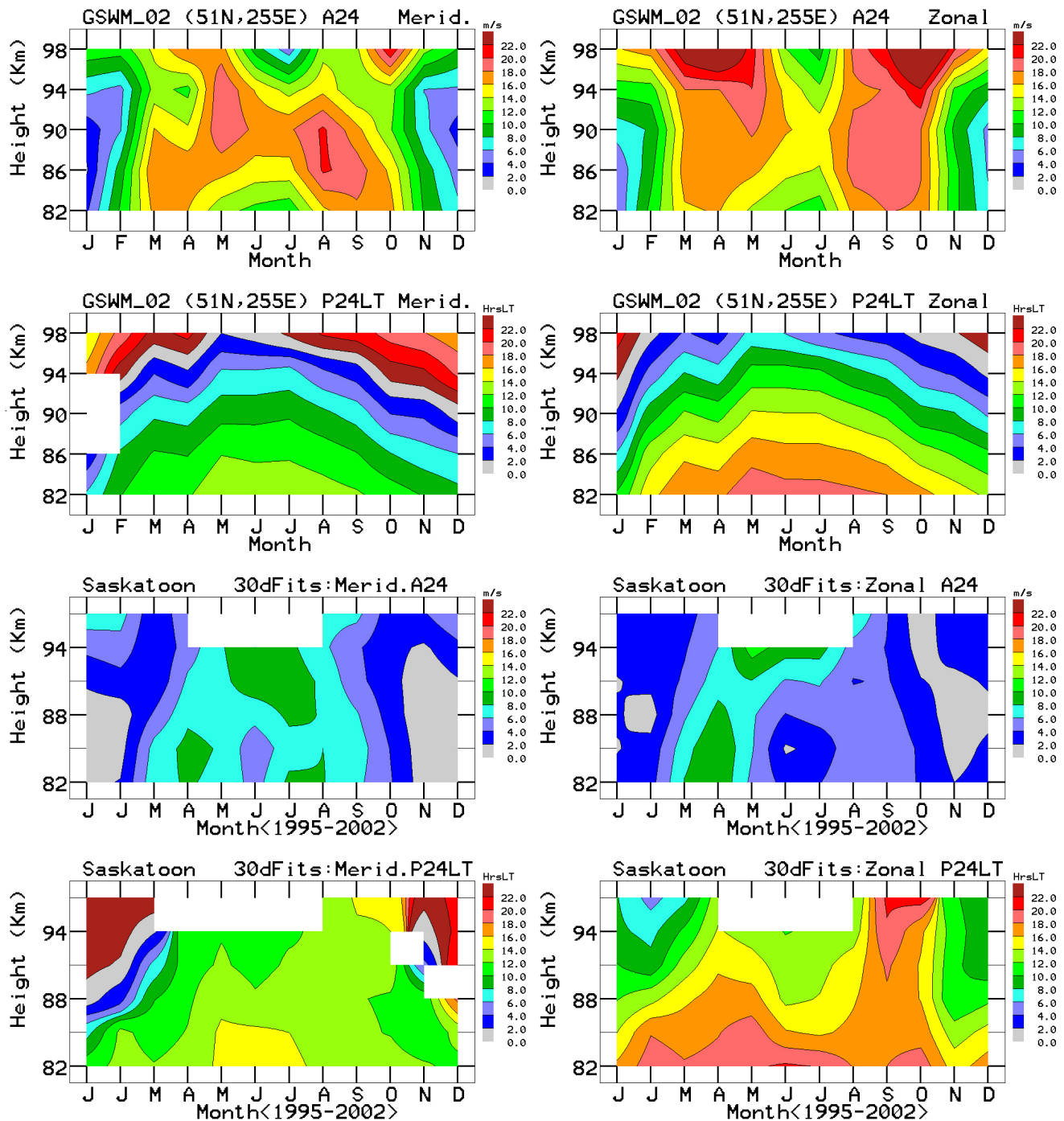
Fig. 5. Climatologies of diurnal tides from GSWM-02 and the Saskatoon MF radar (52 N, 107 W) for 1995–2002.

Scandinavia (Manson et al., 2004b) demonstrated speed ratios of circa 1.5 above 90 km, but with excellent phase/phase-gradient agreements in tides. Thus, the differences in Fig. 5 are not due to those system biases. It must be emphasized that there are inherent limitations to GSWM-02, as discussed in Sects. 1 and 2, since significant sources of nonmigrating tides other than the tropospheric latent heat forcing have been (knowingly) neglected. This can lead to both underestimates and overestimates of the nonmigrating tidal amplitudes (in

comparison with the observed tides), as well as phase discrepancies which can, in turn, affect the longitudinal variability of the modelled MLT tides. The presence of nonmigrating tides from the full variety of sources will also probably affect the vertical structure of the tide, and provide the type of differences in phase gradients already seen between GSWM-00 and GSWM-02 (the vertical wavelengths from the latter at Saskatoon are slightly longer (<10%) than those from the former). These comparisons for the diurnal tide are very

important, as they provide insights as to the possible importance of other sources of nonmigrating tides, and their role in establishing the global structure of the tidal field.

4 Semi-diurnal tides

4.1 HRDI global tides at 96 km

Following Sect. 3, we follow the same pattern of presentation, textually and graphically. In Fig. 6 the dominant spectral features of the spatial spectral analysis of the complex tidal field are centred on s=2; this is the migrating tide, and the feature is broadest at higher latitudes and during the equinox. It does overlap the s=1, 3 positions on occasion, but, as with the diurnal tide, those amplitude components are not resolved. The resolved spectral features are summarized in Table 3 (contours reaching ∼14 dB, yellow), and frequently also include s=−2, 0, 4; during equinox there are additional features at s=−5, −4, 5, 6. As noted in the Introduction, tides or components related to topographic forcing ("wave numbers" of 4 and 1) would include s=−2, 6 and 1, 3 (Forbes et al., 2003), but such tides may or may not reach the MLT with significant amplitude. Nonlinear processes involving the standing planetary waves with wave numbers 1 and 2 would force s=1, 3 (again) and s=0, 4, respectively. Hence, it appears that a selection of the forced nonmigrating tides have reached the MLT.

Consistent with the relatively weak but numerous spectral features other than for s=2, the global longitudinal tidal structures of Fig. 7 are relatively weak or indistinct, which contrasts strongly with the diurnal tide. The number of maxima or features in the amplitude and phase plots ranges from 1 to 3, with a preference for 2 (S=2), as summarized in Table 2. Such preference is consistent with the frequent occurrence of enhanced spectral contours for nonmigrating tides of wave number s=4.

Considering the tidal phases from Fig. 6, the migrating s=2 tide appears to be dominantly symmetric, with usually 0/6 hour phase changes across the equator for the EW/NS wind components. Here the phase values are retained for contours if they have amplitudes above the second colour bin, to minimize noisy values. The corresponding amplitude maxima occur at latitudes poleward of ±24°, indicating the presence of (2, 2) and higher Hough modes (2, 4), etc. There is also evidence for antisymmetric modes as the amplitude minima do not always coincide with the equator, and in the case of June/July (NS component) the phases are continuous across the equator at low latitudes.

The phases for a possible pair of tides with s=1, 3 do not show any systematic variations across the equator (unlike the s=0, 2 pair for the diurnal tide), suggesting that if physically present, their amplitudes are very weak compared with the s=2 migrating tide. Otherwise, the assignment of phase values from Fig. 6 is made problematic by the small amplitudes (5 to 15 dB less than the s=2 features), and the lack of symmetry in spectral amplitudes about the equator. Because of

this, phases are sometimes available in the figure only in one hemisphere at some higher latitude. Mode assignment is therefore difficult or impossible. Considering the s=0, 4 pair, both of which occur in the spatial spectra quite frequently (Table 2), their occurrence as yellow contours within 4–5 colours (10–15 dB) of the maxima is in every case limited to one hemisphere in a narrow latitudinal range. The phases are not available over a sufficient range of latitudes to comment on the tidal mode. Finally, the s=−2, 6 pair do offer more opportunities for hemispheric phase assessments; in December/January and September/October the NS component shows clear continuity of phase at s=−2, suggesting an antisymmetric Hough mode (the EW amplitudes are too small to provide coherent phases).

4.2 GSWM-02 global tides at 94 km

The spatial spectra of the GSWM data in Fig. 8 are visually or qualitatively rather similar to the HRDI spectra (Fig. 6), and there are, relative to the diurnal tide, a larger number of weak spectral features. That being said, the modelled spectral features at s=2 are generally narrower than observed. Several spectral (amplitude) features are evident, including s=−2, 0 and particularly s=6 (this is the maximum s value included in the model). Table 4 indicates the consistent appearance of these features (for the two-month seasons), which is in contrast to Table 3 for HRDI: s=6 is forced consistently and significantly in the model and s=4 quite weakly, while s=4 is preferred observationally. The latter could be due to nonlinear interactions with the standing planetary wave of wave number 2, which are not included in the GSWM-02.

The modelled dominance of the s=6 nonmigrating tide has the expected influence upon the global GSWM tidal amplitude and phase structures of Fig. 9, where the structure number S=4 is dominant in the SH during July (and in months of May–September, not shown). There are also four maxima at equatorial and SH latitudes during October, but that is probably related to the s=−2 wave number spectral peaks (these latter are also increasingly important during the late SH winter and spring in GSWM). Finally, there are four and two structures at low and high latitudes, respectively, during January (and other neighbouring solstitial months), consistent with comparable s=−2, 6 but also s=0 spectral peaks. Such longitudinal structure is not evident in HRDI observations (Fig. 7), where the wave number spectral peaks at s=−2 and particularly at s=6 are relatively weaker (Fig. 6).

Now to continue with phase assessments, the modelled migrating s=2 tide shows consistent evidence (Fig. 8) for the dominance of the symmetric Hough modes ((2, 2) and higher orders during equinoxes) with close to zero or small (∼3 h) phase differences between hemispheres for the EW component and ∼6-h differences for the NS component at high and low latitudes. Here we have again assessed the two month seasonal pairs and not just the plotted months. Again, to emphasize the dominant spectral features, we have shown the phases in Fig. 8 only when the intensity is greater than the second contour. The alternate tendency to symmetry is

Table 3. Summary of HRDI Tidal Components: Semi-Diurnal.

HRDI	NS Wind	EW Wind
December–January 1993/94	4 2 0 −2 −4 (2 longitudinal structures)[c]	4 2 −2 (2 longitudinal structures)[c]
June–July 1993	4 2[a] −2 −4 (1 longitudinal structures)[c]	2[a] −1 −4 (3 longitudinal structures)[c]
September–October 1994	6 5 2[b] 0 −2 −4 −5 −6 (2 longitudinal structures)	6 5 4 2[b] 0 −2 −4 −5 (irregular structures)

[a] Broad feature 1–3, both hemispheres, especially NS component.
[b] Broad feature 1–3, both hemispheres.
[c] HRDI tidal contours (Fig. 7).

Table 4. Summary of GSWM-02 Tidal Components: Semi-Diurnal.

GSWM	NS Wind	EW Wind
December/January	6 2[a] 0 −2 (complex 2, 4 longitudinal structures)[b]	6 2[a] 0 −2 (complex 2, 4 longitudinal structures)[b]
June/July	6 5[W] 4[W] 2[a] 0 −2[W] (complex 2, 4 longitudinal structures)[b]	6 5[W] 4[W] 2[a] 0 −2[W] (complex 2, 4 longitudinal structures)[b]
September/October	6 4[W] 2 0 −2[W] −3[W] −6[W] (complex 2, 4 structures) [b]	6 4[W] 2 0 −2[W] −3[W] −6[W] (complex 2, 4 structures) [b]

[a] Broad feature 1–3, both hemispheres.
[b] GSWM-02 tidal contours (Fig. 9).
[W] Relatively weak, or in one of two months.

for the higher (48–72°) latitudes in June/July and December/January (and neighbouring months), when antisymmetric modal influences (several hours phase differences for EW and NS components) exist. This pattern of phases is also evident in the global tidal structures (Fig. 9), where the phase structures are more continuous across the equator for the EW in all 3 months, while the NS shows discontinuous colour bands. During the solstices the colour contrasts (phase differences) are stronger at high latitudes for the EW component.

When assessing the hemispheric phase differences for the nonmigrating tides the lack of hemispheric symmetry in the occurrence of features above the noise level (typically the light blue and green areas) for several of the tides makes for some difficulty. This was also a problem for HRDI phases (Fig. 6). However, for s=0, and for the available months (mainly solstitial and including the plotted July) the NS hemispheric phase differences of higher latitudes are typically small, with the EW being larger. A combination of antisymmetric modes is favoured. Finally, for the s=−2, 6 pair of nonmigrating tides only the former provided matching hemispheric contours, and then mainly in the equinoctial months. Again, antisymmetric tendencies were quite clear. This result is consistent with HRDI phases for s=−2 in similar months (equinoctial).

Again, in concluding this section, it is valuable to make some general observations about the semidiurnal tide as represented in the global tidal structures from HRDI and the GSWM-02, i.e. the dominant migrating tidal characteristics. Thus, we compare Figs. 7 and 9. For the solstices the main modelled characteristic is for strong amplitude maxima in the local winter hemisphere poleward of 30 degrees latitude. The HRDI amplitudes are less dominated by the winter, and the observed summer values are much larger (circa 20 m/s) than modelled (0–10 m/s). That being said, the colour contours of phases are rather similar for GSWM-02 and HRDI at this altitude, especially where the winter amplitudes maximize. During October, GSWM-02 demonstrates strong symmetry of (small) amplitudes about the equator, with consistent phases. The observed amplitudes and phases are rather different: amplitudes are much larger (20–50 m/s versus 5–20 m/s), and phases/colours and patterns differ.

Hence, we show the last figure of the comparisons (Fig. 10) with radar and GSWM climatologies for the Saskatoon mid-latitude location, where the 12-h tidal characteristics are well displayed (Manson et al., 2002a). As expected from the previous discussion, the modelled amplitudes are smaller than the MF radar values everywhere but during winter. There, and allowing for the 1.5 speed factor
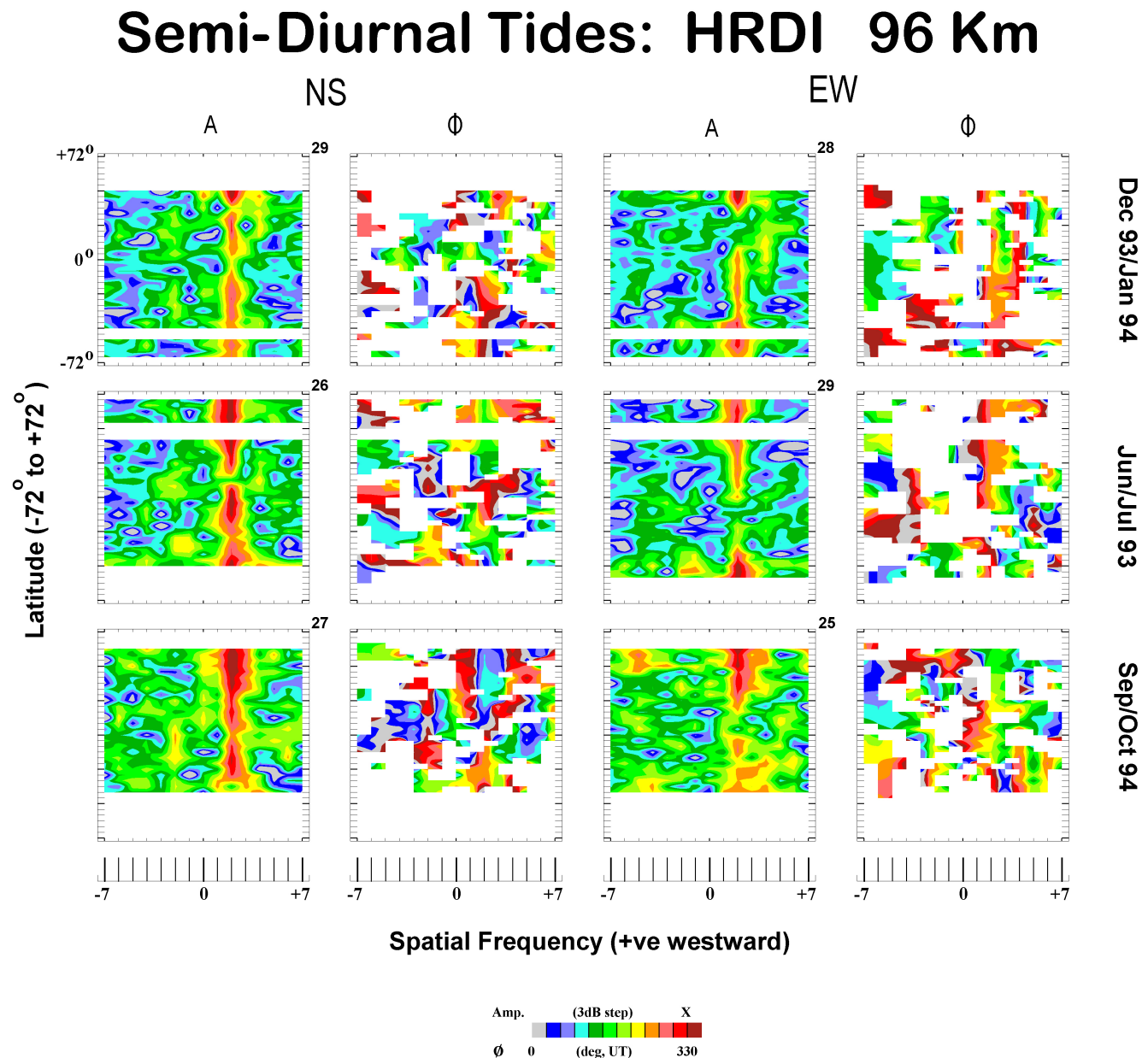
Semi-Diurnal Tides: HRDI 96 Km

Fig. 6. Spatial spectral analysis of the global HRDI complex semidiurnal wind field, providing wave number versus latitude contours of amplitude and phase. Otherwise the description is as for Fig. 1.

adjustment, the values are similar. Equivalent vertical wavelengths, are ∼65 km in GSWM-02 and ∼45 km for the MFR, but phases/colours are similar near 90 km. Otherwise, the observed dominant autumn feature is not reproduced, nor the smaller spring feature. At these times and in the summer, the observed phases and their gradients (longer wavelengths) are also quite dissimilar.

In the present context, the addition of the 12-h tidal components forced by tropospheric latent heat has provided modelled values (GSWM-02) for a mid-latitude location that are modestly different from those of GSWM-00 (Manson et al., 2002a, 2003): the amplitudes of GSWM-02 are larger by circa 10%, and the vertical wavelengths while generally

similar, are shorter in May and June. In these studies the GSWM-00 version has already been shown to have significant differences from observations in this regard. Models with tidal forcing due to nonlinear interactions with standing planetary waves hold the prospect for better agreement, as do models with longitudinally varying ozone distributions. Otherwise, the comments made in the conclusion of Sect. 3 regarding the inherent limitations to GSWM-02, also apply here. In this regard the 12-h tides in the Canadian (General Circulation) Middle Atmosphere Model (CMAM) were fairly realistic (Manson et al., 2002c), and experiments using the interactive chemistry software for that model are underway.
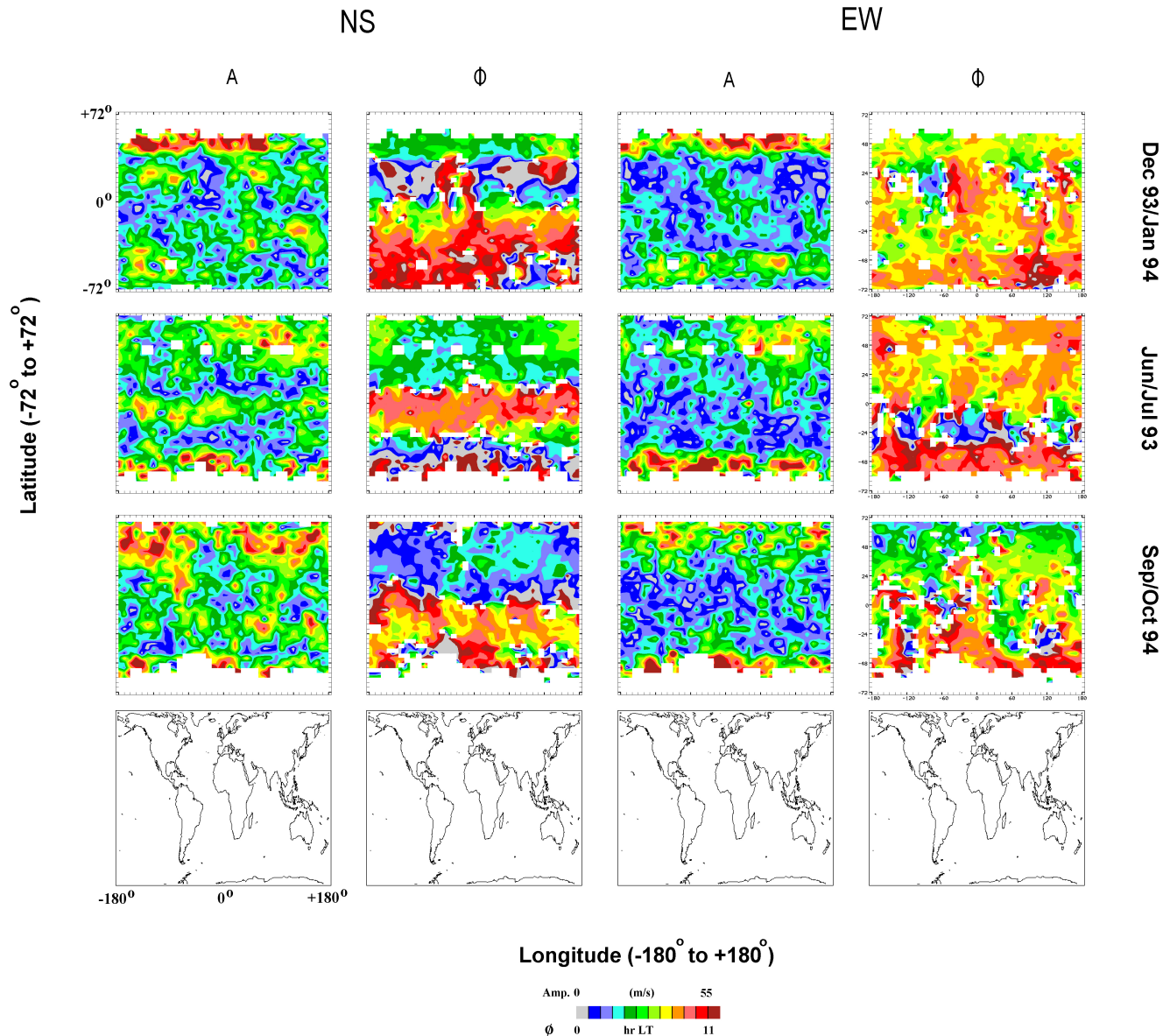
Global HRDI Tidal Structures: Semi-Diurnal 96 Km

Fig. 7. Global HRDI tidal structures for the semidiurnal tide at 96 km, as functions of latitude and longitude. The amplitude increment for each colour is 5 m/s. Otherwise, the description is as for Fig. 2.

5 Summary and conclusions

Following the publication of global HRDI tidal structures (Manson et al., 2002a) that demonstrated significant longitudinal variations in the global distribution of amplitudes and phases of the 12-h and especially the 24-h tides, it was appropriate to assess the spatial tidal frequencies (or wave numbers) inherent in those structures. The development of the GSWM-02, which now contains migrating and nonmigrating tides (or components), has also provided the opportunity for modelling comparisons (Hagan and Forbes 2002, 2003).

Considering the diurnal tide, the HRDI spatial spectra (plots of wave number versus latitude) for the 3 seasons (both solstices and the September/October equinox) were dominated by a broad feature centered on wave number 1 (s=1) and stretching from s=0–2. The global phases and amplitudes were consistent with the symmetric migrating (1, 1) Hough mode, and with symmetric and antisymmetric modes for nonmigrating tides having values of s=2 and s=0, respectively, as suggested by Forbes et al. (2003). Otherwise, the s=−3 tide in the EW wind component was spectrally strong in the June/July and September/October seasons, which,

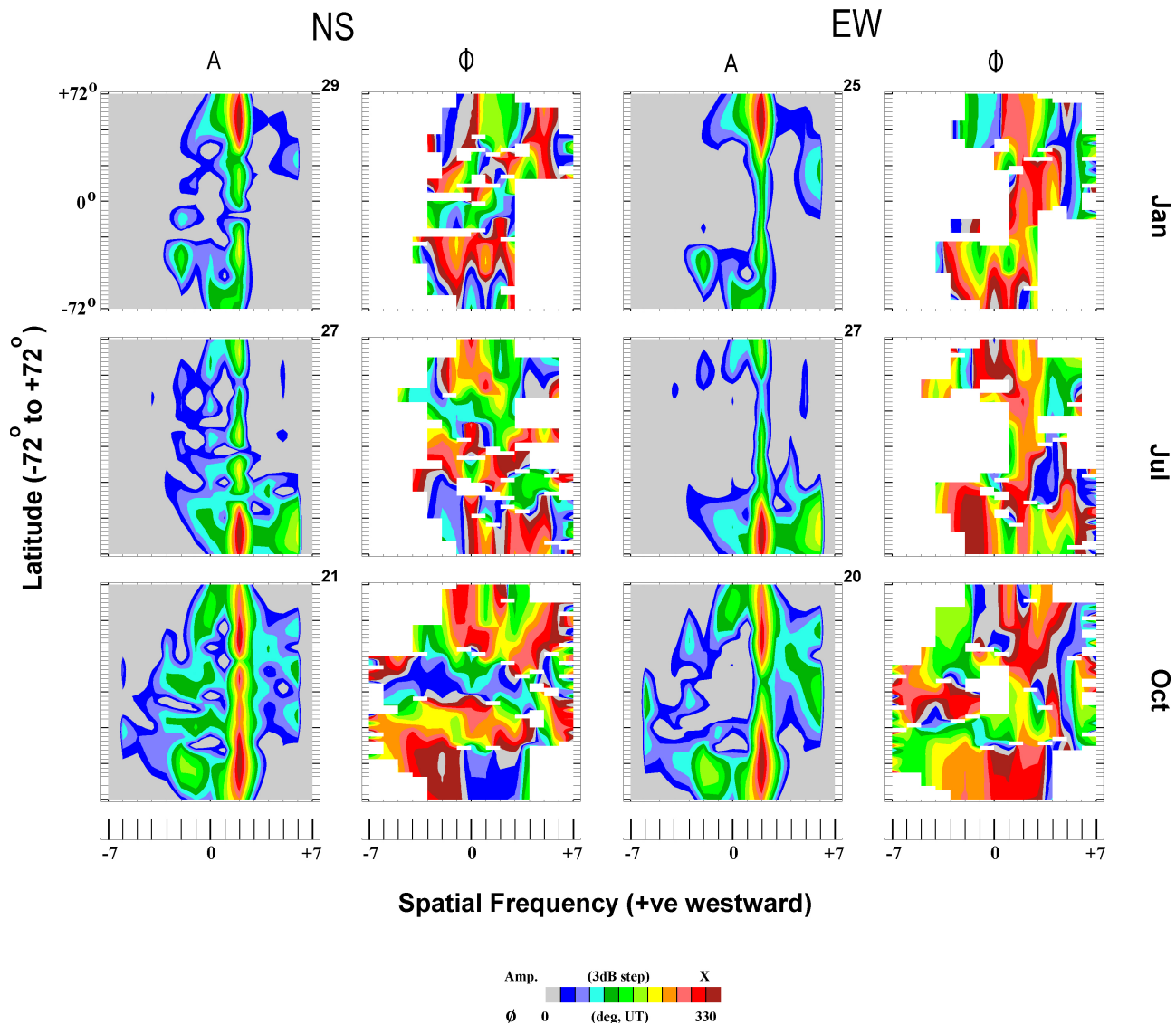# Semi-Diurnal Tides: GSWM 94 Km

Fig. 8. Spatial spectral analysis of the global GSWM-02 complex semidiurnal wind field, providing wave number versus latitude contours of amplitude and phase. Otherwise, the description is as for Fig. 1.

combined with the dominant s=1 tide, was consistent with four maxima in the global longitudinal tidal structures. (The number of maxima, or the structure number S, is given by the difference between the wave number of the migrating tide and that of the nonmigrating tide.) Phases then favoured the symmetric Kelvin wave. The s=−3 was also evident in the December/January NS component.

The GSWM spatial spectra for the diurnal tide were generally rather similar, with dominant intensities at wave numbers s=−3, 1. However, the s=1 spectral feature for the (1, 1) symmetric Hough mode was not as broad, and there was, therefore, no evidence for unique phases for s=0, 2; and the tide appropriate to the s=−3 spectral feature was more consistently modelled than observed. This latter led to clear global longitudinal tidal structures (S=4) in all 3 sea-

sons (EW wind component) and additionally for the NS wind component in December/January. Consistent with the existence of topographical features of "wave number" 4, the tidal structures tended to be aligned with the oceans. (This association was also evident for the observed tidal structures, although there it was weaker and limited to the EW component.) The Kelvin wave mode was again favoured for June/July and September/October, while phases favoured an antisymmetric Hough mode in December/January (as was the case for HRDI). The nonmigrating tide with s=4 in the model was more evident than in observations.

Overall, the nonmigrating tides forced by solar heating associated with deep convection (s=−3 and 0, 2) appear to be the dominant MLT tides in HRDI and GSWM-02 (also based on Hagan and Forbes, 2002) with no evidence in HRDI

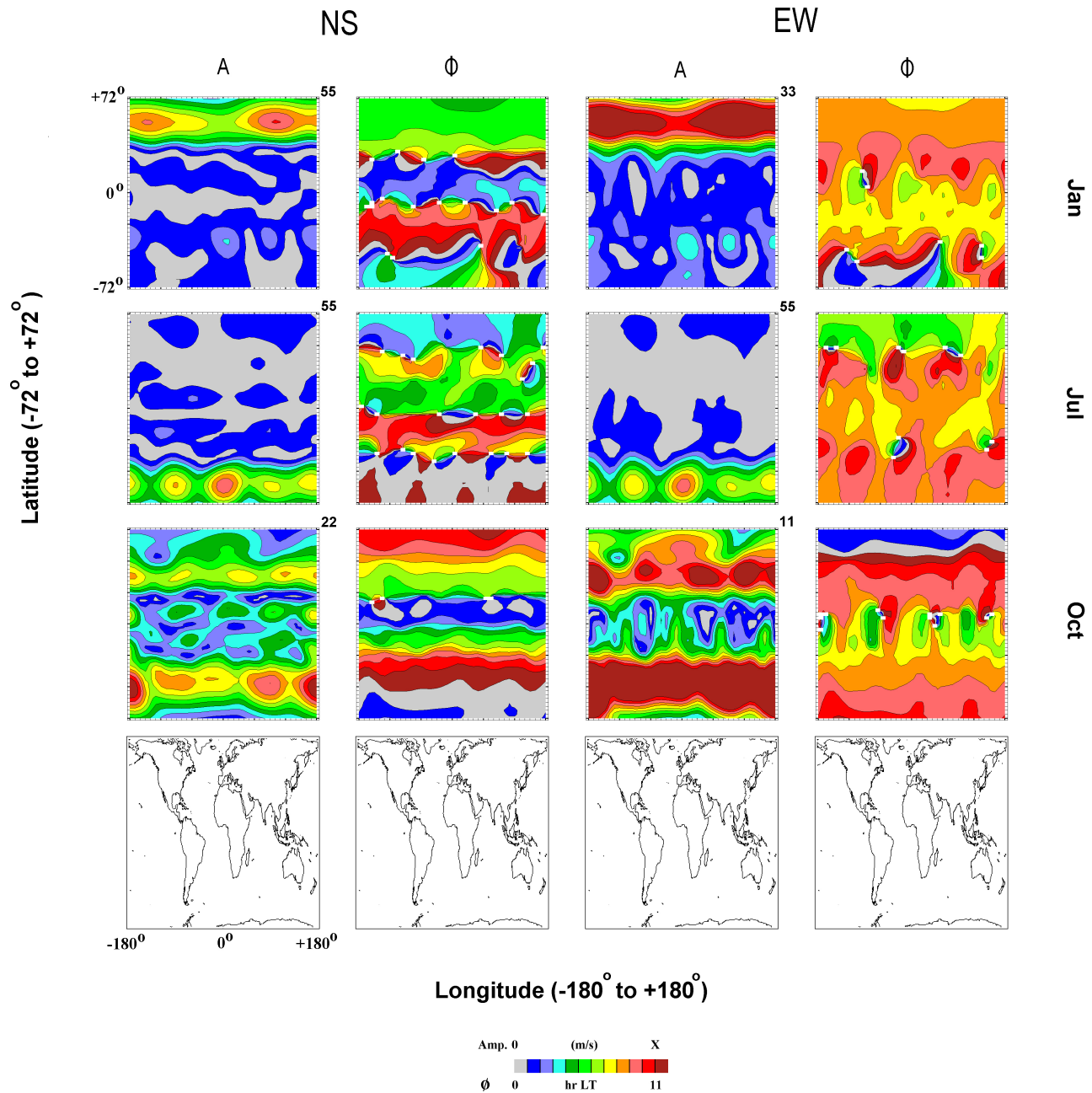# Global GSWM Tidal Structures: Semi-Diurnal 94 Km

Fig. 9. Global GSWM-02 tidal structures for the semidiurnal tide at 96 km, as functions of latitude and longitude. The amplitude increments for each colour are 1, 2, 3, or 5 m/s, respectively. Otherwise, the description is as for Fig. 2.

data for the s=−1, 3 tides associated with nonlinear interactions with the standing planetary wave of wave number two. (However, the observed s=0, 2 tides could also be associated with the planetary wave of wave number one.) Differences in the observed and modelled tidal spatial (amplitude) spectra and complementary global tidal structures led to careful inspection of the overall (average) global tidal structures at 94–96 km. The equinoctial maxima at 94 km in the model are large and exceed the HRDI values, especially at lati-

tudes poleward of 40°. This is unlike the GSWM-95 values (Manson et al., 2002a). Consistent with that, comparisons of annual MLT climatologies (82–97/8 km) of monthly amplitudes and phases from the Saskatoon MF radar and from GSWM-02 for 52/51° N and 107/105° W reveal significant differences. Equinoctial maxima, and short vertical wavelengths are a strong modelled feature, while much longer wavelengths and summer maximum are observed.
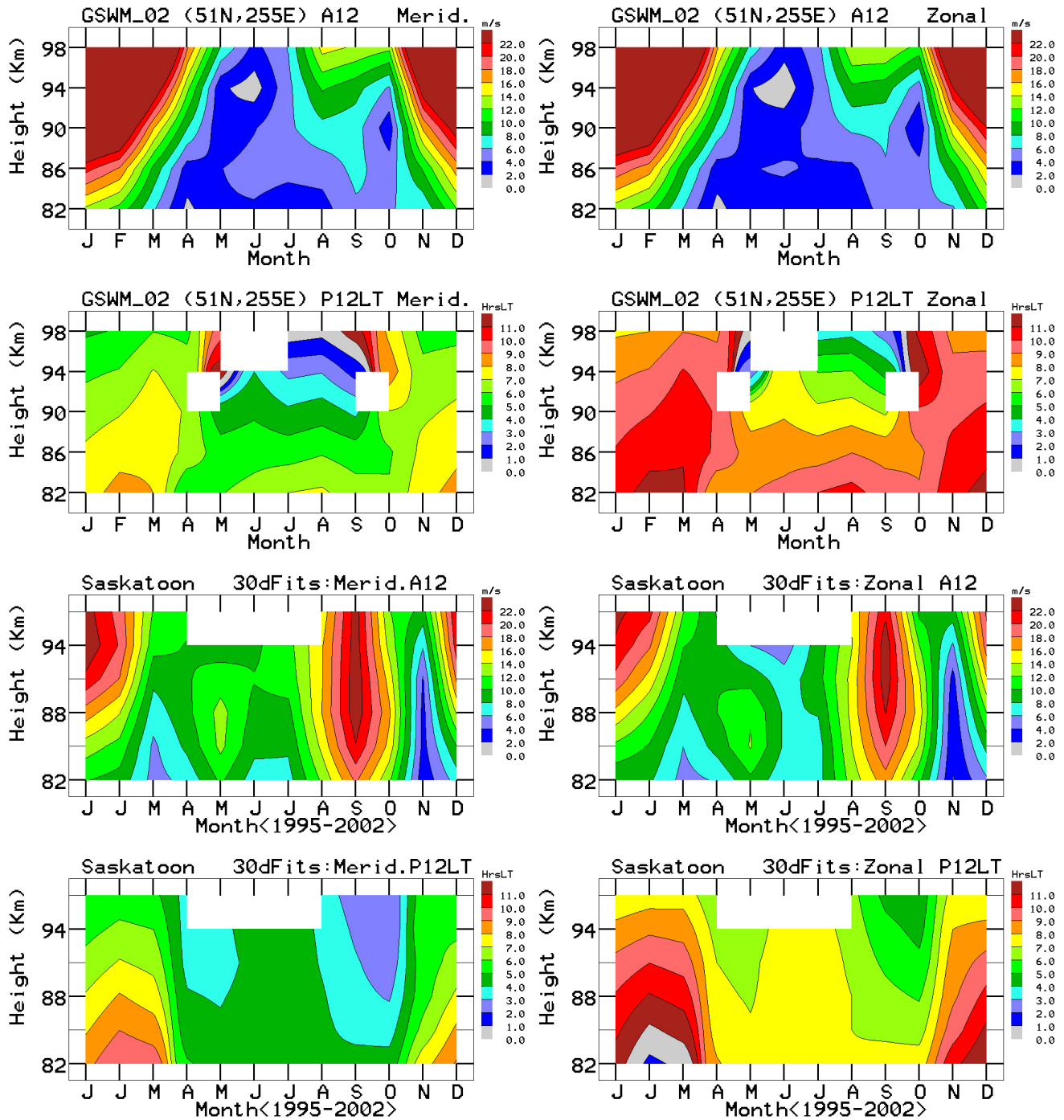
Fig. 10. Climatologies of semidiurnal tides from GSWM-02 and the Saskatoon MF radar (52 N, 107 W) for 1995–2002.

The spatial spectra for the semidiurnal tides within the HRDI data provided even more evidence for a range of non-migrating tides, although their amplitudes were weak compared with the migrating tide. The latter was dominated by symmetric Hough modes, e.g. (2, 2), (2, 4), etc. The most frequently observed nonmigrating tides were of wave number s=−2, 0, 4; the first could be due to topographic forcing at "wave number" four, and the latter two by nonlinear processes involving the standing planetary wave of wave number

2. Consistent with the weak spectral features for the non-migrating tides, the global longitudinal tidal structure was only weakly modulated, with a slight preference for structure number 2 due to the beating of the migrating tide (s=2) with the nonmigrating s=4 tide. Phases for those weak tides were seldom defined above noise levels in both hemispheres and hence tidal modes could not usually be determined. Phases for the s=−2 tide had some antisymmetric tendencies.

The GSWM spatial spectra (12-h tide) provided less seasonal variation than the HRDI spectra, and with more frequent and intense spectral features due to certain nonmigrating tides (s=−2, 0, 6). Each season and component then consistently demonstrated strong structures in the global longitudinal tide (two or four maxima). The s=6 tide is strongly forced by the deep convection processes in the model, whereas forcing for s=4 (seen in HRDI) is clearly weaker in the model. There were some indications that the s=−2, 0 tides are due to antisymmetric Hough modes. Migrating tides (s=2) again provided phases consistent with symmetric Hough modes (2, 2) and higher orders, especially at low and middle latitudes, but antisymmetric mode tendencies increased beyond 48°.

Differences in the tidal spatial spectra between HRDI and GSWM-02 led to careful scrutiny of the average global tidal structures. The main differences are that the model shows strong annual dominance of the winter tide poleward of 30° latitude, whereas the observed summer and equinoctial amplitudes are closer to their winter amplitudes. Comparisons between annual climatologies (82–97/8 km) for the mid-latitude (52° N) Saskatoon MF radar and GSWM-02 revealed these seasonal differences throughout the MLT, and in addition, demonstrated the observed equinoctial maxima (especially in autumn). Vertical wavelengths differed most strongly, as expected, in non-winter months, with larger observed values. Models with standing planetary waves, and with alternate ozone distributions (including longitudinal variations), have the potential to provide 12-h tides in closer agreement with observations. Longitudinal variations in GSWM-02 are quite significant in the winters poleward of 40°, but this does not alter the above generalizations.

Given the significant differences between the observed and modelled migrating and nonmigrating tides, it seems appropriate here to stress the comments made earlier regarding the following inherent and recognized limitations to GSWM-02. The model was developed to explore the effects of tropospheric latent heat processes upon the spatial spectra of nonmigrating tides. It was realized that other heating mechanisms, such as the insolation absorption by longitudinally varying water vapour and ozone, will also be important. There are also PW and GW interactions with tides to be considered e.g. McLandress and Ward (1994), and Hagan and Roble (2001). These comparisons have shown that other tidal forcings may indeed be required before very good agreement between observations and GSWM modelling is achieved. Additional nonmigrating tides forced by these various mechanisms will lead to differences in the modelled longitudinal, latitudinal and altitudinal structures of the total tidal fields. With regard to GSWM-02 itself, we stress that more global comparisons with observations are needed. In particular, tidal temperatures are needed, as their distribution differs strongly from that of the two wind components. Studies are also desirable at higher latitudes than available here from HRDI.

In conclusion, the important role of nonmigrating solar tides in descriptions of the MLT tidal fields has been clearly illustrated using global HRDI and GSWM-02 data from near 95 km. The nonmigrating tides lead to strong longitudinal variations or structures in the total tidal fields of amplitudes and phases, especially for the diurnal tide. These variations should be considered when comparisons are made between ground-based observations. Such structures will also play an important role in determining the regional relationships between interacting waves, such as gravity, planetary and tidal waves.

References

Angelats i Coll, M. and Forbes, J. M.: Nonlinear interactions in the upper atmosphere: the s=1 and s=3 nonmigrating semidiurnal tides, J. Geophys. Res., 107, (A8), SIA3, doi: 10.1029/2001JA900179, 2002.

Fomichev, V. I., Ward, W. E., Beagley, S. R., McLandress, C., McConnell, J. C., McFarlane, N. A., and Shepherd, T. G.: Extended Canadian Middle Atmosphere Model: Zonal-mean climatology and physical parameterizations, J. Geophys. Res., 107, (D9–10), ACL9, doi: 10.1029/2001JD000479, 2002.

Forbes, J. M., Zhang, X., Talaat, E. R., and Ward, W.: Nonmigrating diurnal tides in the thermosphere, J. Geophys. Res., 108, (A1), SIA7, 1033, doi: 10.1029/2002JA009262, 2003.

Forbes, J. M., Zhang, X., and Hagan, M.E.: Simulations of diurnal tides due to tropospheric heating from the NCEP/NCAR Reanalysis Project, Geophys. Res. Lett., 28, 3851–3854, 2001.

Forbes, J. M., Hagan, M. E., Zhang, X., and Hamilton, K.: Upper-atmosphere tidal oscillations due to latent heat release in the tropical troposphere, Ann. Geophys., 15, 9, 1165, 1997.

Hagan, M. E. and Forbes, J. M.: Migrating and nonmigrating semidiurnal tides in the upper atmosphere excited by tropospheric latent heat release, J. Geophys. Res., 108, (A2), SIA6, 1062, doi: 10.1029/2002JA009466, 2003.

Hagan, M. E. and Forbes, J. M.: Migrating and nonmigrating diurnal tides in the middle and upper atmosphere excited by tropospheric latent heat release, J. Geophys. Res., 107, (D24), ACL6, 4754, doi: 10.1029/2001JD001236, 2002.

Hagan, M. E. and Roble, R. G.: Modeling diurnal tidal variability with the NCAR TIME-GCM, J. Geophys. Res., 106, 24 869–24 882, 2001.

Hagan, M. E., Roble, R. G., and Hackney, J.: Migrating thermospheric tides, J. Geophys. Res., 106, 12 739–12 752, 2001.

Jacobi, Ch., Portnyagin, Y. I., Solovjova, T. V., Hoffman, P., Singer, W., Fahrutdinova, A. N., Ishmuratov, R. A., Beard, A. G., Mitchell, N. J., Muller, H. G., Schminder, R., Kurschner, D., Manson, A. H., and Meek, C. E.: Climatology of the semidiurnal tide at 52–56N from ground-based radar wind measurements 1985–1995, J. Atmos. Solar-Terr. Phys. 61, 975–991, 1999.

Llewellyn, E. J.: The Odin aeronomy mission, Can J. Phys., 80, (4), VII–VIII APR 2002.

Manson, A. H., Meek, C. E., Chshyolkova, T., Avery, S. K., Thorsen, D., MacDougall, J. W., Hocking, W., Murayama, Y.,

Igarashi, K., Namboothiri, S. P., and Kishore, P.: Longitudinal and Latitudinal Variations in Dynamic Characteristics of the MLT (70–95 km): A study involving the CUJO network, Ann. Geophys., 22, 347–365, 2004a.

Manson, A. H., Meek, C. E., Avery, S. K, and Thorsen, D.: Ionospheric and Dynamical characteristics of the MLT region over Platteville (40° N, 105° W) and Comparisons with the region over Saskatoon (52° N, 107° W), J. Geophys. Res., 108, (D13), ACL12, 2003.

Manson, A. H., Meek, C. E., Hall, C. M., Nozawa, S., Mitchell, N. J., Pancheva, D., Singer, W., and Hoffmann, P.: Mesopause Dynamics from the Scandinavian Triangle of Radars within the PSMOS-DATAR Project, Ann. Geophys., 22, 367–386, 2004b.

Manson, A. H., Meek, C. E., Hagan, M., Koshyk, J., Franke, S., Fritts, D., Hall, C., Hocking, W., Igarashi, K., MacDougall, J., Riggin, and D., Vincent, R.: Seasonal Variations of the Semi-Diurnal and Diurnal Tides in the MLT: Multi-Year MF Radar Observations from 2–70° N, Modelled Tides (GSWM, CMAM), Ann. Geophys., 20, 661–667, 2002a.

Manson, A. H., Luo, Y., and Meek, C.: Global Distributions of Diurnal and Semi-Diurnal Tides: Observations from HRDI-UARS of the MLT Region, Ann. Geophys., 20, 1877–1890, 2002b.

Manson, A. H., Meek, C. E., Koshyk, J., Franke, S., Fritts, D., Riggin, D., Hall, C., Hocking, W., MacDougall, J., Igarashi, K., and Vincent, B.: Gravity Wave Activity and Dynamical effects in the Middle Atmosphere (60–90 km): Observations from an MF/MLT Radar Network, and results from the Canadian Middle Atmosphere Model (CMAM), J. Atmos. Solar-Terr. Phys., 64, 65–90, 2002c.

McLandress, C., Shepherd, G. G., and Solheim, B. H.: Satellite observations of thermospheric tides: results from the wind imaging interferometer on UARS, J. Geophys. Res., 101, 4093–4114, 1996.

McLandress, C. and Ward W. E.: Tidal Gravity-Wave Interactions and their Influence on the Large-Scale Dynamics of the Middle Atmosphere- Model results, J. Geophys. Res., 99, (D4), 8139–8155, 1994.

Pancheva, D., Mitchell, N. J., Hagan, M. E., et al.: Global scale tidal structure in the mesosphere and lower thermosphere during the PSMOS campaign of June–August 1999 and comparisons with the global scale wave model, J. Atmos. Solar-Terr. Phys., 64, 1011–1035, 2002.

Talaat, E. R. and Lieberman, R. S.: Non-migrating Diurnal Tides in the Mesospheric and Lower-Thermospheric Winds and Temperatures, J. Atmos. Sci., 24, 4073–4087, 1999.

Yagai, I.: Non-migrating thermal tides detected in data analysis and a general circulation model simulation, J. Geophys. Res., 94, 6341–6356, 1989.